Atmos. Chem. Phys. Discuss., https://doi.org/10.5194/acp-2018-110
Manuscript under review for journal Atmos. Chem. Phys.
Discussion started: 12 April 2018

Atmospheric Chemistry and Physics Discussions

Intra-annual variations of regional aerosol optical depth, vertical distribution, and particle types from multiple satellite and ground-based observational datasets

Bin Zhao[1], Jonathan H. Jiang[2], David J. Diner[2], Hui Su[2], Yu Gu[1], Kuo-Nan Liou[1], Zhe Jiang[1], Lei Huang[1], Yoshi Takano[1], Xuehua Fan[1], and Ali H. Omar[3]

[1]Joint Institute for Regional Earth System Science and Engineering and Department of Atmospheric and Oceanic Sciences, University of California, Los Angeles, California, USA.
[2]Jet propulsion Laboratory, California Institute of Technology, Pasadena, California, USA.
[3]NASA Langley Research Center, Hampton, Virginia, USA.

Corresponding author: Bin Zhao (zhaob1206@ucla.edu)

Atmos. Chem. Phys. Discuss., https://doi.org/10.5194/acp-2018-110
Manuscript under review for journal Atmos. Chem. Phys.
Discussion started: 12 April 2018

Atmospheric Chemistry and Physics Discussions

Abstract

The relatively short lifetimes of aerosols in the atmosphere result in climatic and health effects that are strongly dependent on intra-annual variations in particle concentrations. While many studies have examined the seasonal and diurnal variations of regional aerosol optical depth (AOD), understanding the temporal variations in aerosol vertical distribution and particle types is also important for accurate computation of aerosol radiative effects. In this paper, we combine the observations from four satellite-borne sensors and ground-based AOD and fine particle ($PM_{2.5}$) measurements to investigate the seasonal and diurnal variations of aerosol column loading, vertical distribution, and particle types over three populous regions: the Eastern United States (EUS), Western Europe (WEU), and Eastern and Central China (ECC). In all three regions, column AOD, as well as AOD higher than 800 m above ground level, peaks in summer/spring probably due to accelerated formation of secondary aerosols and hygroscopic growth. However, AOD at height below 800 m mostly peaks in winter except that a second maximum in summer occurs over the EUS region, which is consistent with observed temporal trends in surface $PM_{2.5}$ concentrations. AOD due to fine particles (< 0.7 μm diameter) is much larger in spring/summer than in winter over all three regions, whereas coarse mode AOD (> 1.4 μm diameter) generally shows less variability, except for the ECC region where a peak occurs in spring, consistent with the prevalence of airborne dust during this season. When aerosols are classified according to sources, the dominant type is associated with anthropogenic air pollution, which has a similar seasonal pattern as total AOD. Dust and sea-spray aerosols in the WEU region peak in summer and winter, respectively, but do not show an obvious seasonal pattern in the EUS region. Smoke aerosols, as well as absorbing aerosols, present an obvious unimodal distribution with a maximum occurring in summer over the EUS and WEU regions, whereas they follow a bimodal

distribution with peaks in August and March (due to crop residue burning) over the ECC region. In general, the nighttime-daytime AOD difference is more positive in summer than in winter, likely attributable to a larger diurnal temperature range in summer. Smoke AOD is much higher in the nighttime than in the daytime. The results of this study can help to improve the current estimates of the climatic and health impacts of aerosols.

1 Introduction

Aerosols have adverse effects on human health (Lelieveld et al., 2015) and play a key role in Earth's climate through aerosol-radiation interactions (McCormick and Ludwig, 1967) and aerosol-cloud interactions (Twomey, 1977; Albrecht, 1989; Garrett and Zhao, 2006). Compared with long-lived climate forcers such as CO_2, aerosols have relatively short lifetimes and hence large spatiotemporal variability (Unger et al., 2008; Shindell et al., 2009). While the climatic effects of CO_2 are mainly induced by inter-annual concentration changes, the climatic and health effects of aerosols also strongly depend on their intra-annual (seasonal and diurnal) variability.

Aerosol optical depth (AOD) has been widely used to represent the column aerosol loading and to assess the aerosol impacts on radiation, clouds, and precipitation (Ma et al., 2014; Niu and Li, 2012; Zhao et al., 2018; Song et al., 2017). However, the wide ranges of particle scattering and absorption properties mean that even for the same AOD, different aerosol components have different effects on not only the magnitude, but also the sign, of aerosol radiative forcing (IPCC, 2013; Gu et al., 2006). IPCC (2013) estimates that the historical global mean direct radiative forcings due to sulfate, organic carbon (OC), black carbon (BC), and mineral dust are −0.40, −0.19, +0.36, and −0.10 W m^{-2}, respectively. Furthermore, absorbing

and non-absorbing aerosols have been found to have very different impacts on the development of convective clouds (Massie et al., 2016; Ramanathan et al., 2005; Rosenfeld et al., 2008). Besides aerosol type, perturbation of aerosol vertical distribution influences the vertical profile of heating rate (Johnson et al., 2008; Guan et al., 2010; Zhang et al., 2013), which subsequently modifies the atmospheric stability and convective strength (Ramanathan et al., 2007), with potential changes in regional circulation (Ramanathan et al., 2001) and cloud cover (Johnson et al., 2004). Understanding aerosol variability as a function of height is also important because the health impacts of aerosols are only associated with those present near the surface, where they are inhaled. For these reasons, systematic analyses of the intra-annual variations of aerosol vertical distribution and particle types, in addition to total column AOD, are necessary to improve our understanding of aerosol climatic and health effects.

Numerous studies have investigated the seasonal variations of AOD at global and regional scales using satellite observations (e.g., Kim et al., 2007; Song et al., 2009; Mehta et al., 2016; Mao et al., 2014). By comparison, most previous studies of the temporal variations of aerosol vertical distributions and aerosol types have been confined to only a few sites due to coverage limitations associated with reliance on ground-based instruments (e.g., Liu et al., 2012; Matthias et al., 2004). Despite continuous advancement of remote sensing technology and emergence of new spaceborne sensors, only limited number of studies have utilized satellite observations to examine the seasonal and/or diurnal variations of aerosol profiles and/or types at regional or larger scales (Huang et al., 2013; Kahn and Gaitley, 2015; Yu et al., 2010; Li et al., 2016). Huang et al. (2013) analyzed the seasonal and diurnal variations of aerosol extinction profile and type distribution using 5-year observations from the Cloud-Aerosol Lidar and Infrared Pathfinder Satellite Observations (CALIPSO). Kahn and Gaitley (2015) examined the

spatiotemporal variations of aerosol types retrieved by the Multi-angle Imaging SpectroRadiometer (MISR). Different satellite-borne sensors, such as MISR, CALIPSO, and Moderate resolution Imaging Spectroradiometer (MODIS), employ different principles of measurement and retrieval, and therefore provide different sensitivities to column AOD, aerosol types, and vertical profiles. Therefore, integration of data from multiple satellites and ground-based observational networks makes it possible to deepen our understanding of the intra-annual variations of aerosol loadings, profiles, and types.

In this study, we investigate the seasonal and diurnal variations of aerosol column loading, vertical distribution, and particle types using multiple satellite and ground-based observational datasets covering the period from 2007 to 2016. The purpose is to assess the consistency among various datasets and provide a comprehensive characterization of aerosol properties in polluted regions to facilitate future studies of aerosol climate effects and local air quality issues. The data are from MISR, MODIS, CALIPSO, Aerosol Robotic Network (AERONET), and surface $PM_{2.5}$ monitors. Consistent with our previous study (Zhao et al., 2017), we selected three populous regions which have experienced substantial anthropogenic pollution (Wang et al., 2017; Wang et al., 2014) and have received considerable attention in other climate studies: the Eastern United States (EUS; 29º-45º N, 70º-98º W), Western Europe (WEU; 37º-59º N, 10º W-17º E), and Eastern and Central China (ECC; 21º-41º N, 102º-122º E). The geographical boundaries of these regions are shown in Fig. 1.

2 Data and Methods

2.1 Satellite data

We obtain retrievals of total column AOD as well as AOD for various height ranges and aerosol types from MISR (flying on the Terra satellite), MODIS (Terra and Aqua), and the Cloud-Aerosol Lidar with Orthogonal Polarization (CALIOP) on CALIPSO.

MISR observes the Earth with moderately high spatial resolution (275 m to 1.1 km) at 9 along-track viewing angles in each of 4 visible/near-infrared spectral bands, which enables the partitioning of AOD by particle type over both land and ocean, in addition to retrieval of total AOD (Kahn and Gaitley, 2015; Kahn et al., 2001). Its observations provide near-global coverage every 9 days (Diner et al., 1998). We make use of the Level 3 monthly global aerosol product (MIL3MAE) version F15_0031, which is generated at a spatial resolution of 0.5° × 0.5°. The variables used in the analysis are total AOD at 555 nm as well as AODs for six aerosol components, namely small (< 0.7 μm diameter), medium (0.7-1.4 μm diameter), large (> 1.4 μm diameter), spherical, non-spherical, and absorbing. Based on comparison with ground-based AERONET measurements, the errors in MISR AOD data are on the order of ±0.05 or ±(0.20 × AOD), whichever is larger (Kahn et al., 2005; Kahn et al., 2010). In addition, retrieval of MISR particle property information from individual retrievals is considered to be reliable when AOD > 0.15, and has diminished sensitivity at smaller AOD (Kahn and Gaitley, 2015; Kahn et al., 2010). In this study we use only monthly mean values, for which the uncertainties are expected to be smaller than those for individual retrievals. Note that we did not do a relative humidity (RH) correction to AOD retrievals from MISR as well as other sensors. The seasonal and diurnal variations of AOD represent an integrated effect of variations in aerosol abundance, vertical distribution, chemical constituents, and meteorological conditions.

The MODIS sensors onboard the Terra and Aqua satellites observe the Earth with multiple wavelength bands over a 2330 km swath (King et al., 2003), which provides near-daily global coverage. In this study we obtain column AOD data at 550 nm with a 1° × 1° resolution from the Level 3 monthly atmosphere products Collection 6 (MOD08 and MYD08 for the Terra and Aqua platforms, respectively). Comparison studies with AERONET have estimated the accuracy of AOD retrievals to be about ±(0.05 + 0.15 × AOD) over land and ±(0.03 + 0.05 × AOD) over ocean (Levy et al., 2010; Remer et al., 2005). For both MISR and MODIS data, we calculate regional mean AOD by averaging valid AOD values over all grids within the three target regions.

CALIOP is a dual-wavelength polarization lidar on the CALIPSO satellite, and is designed to acquire vertical profiles of aerosols and clouds at 532 and 1064 nm wavelengths during both day and night [Winker et al., 2007]. CALIPSO flies in formation with Aqua, and all three satellites employed in this paper fly in orbits having 16-day repeat cycles. In addition to vertical extinction profiles, CALIPSO categorizes an aerosol layer as one of seven types based on a number of parameters including altitude, location, surface type, volume depolarization ratio, and integrated attenuated backscatter [Omar et al., 2009]. The seven aerosol types are dust, smoke, clean continental, polluted continental, polluted dust, clean marine, and dusty marine. For most profiles, this aerosol classification is consistent with that derived from AERONET inversion data (Mielonen et al., 2009). In this study, we adopt the Level 2 aerosol profile product (05kmAPro, V4.10), which has an along-track horizontal resolution of 5 km and a vertical resolution of 60 m or 180 m, depending on whether the aerosol height is below or above 20.2 km altitude. We do not use the CALIOP Level 3 product because it is difficult to collocate with AERONET observations (see Section 2.2) due to its coarse resolution (2° × 5°). For each clear-

sky profile, we calculate the column AOD at 532 nm by vertically integrating extinction coefficients of the features that are identified as "aerosols" and have valid quality control (QC) flags, i.e., -100 ≤ cloud aerosol discrimination (CAD) score ≤ -20, extinction QC = 0/1, and extinction coefficient uncertainty < 99.9 (Huang et al., 2013). In addition, we employ two quality filters used in generating the Level 3 product in order to eliminate features that probably suffer from surface contamination, i.e., near-surface features with large negative extinction coefficients and contaminated features beneath the surface-attached opaque layer (NASA CALIPSO team, 2011). Following the same method, we also bin the 532 nm AODs into various height ranges above ground level (0-200 m, 200-500 m, 500-800m, 800-1200 m, 1200-2000 m, and > 2000 m above the surface elevation) for the individual aerosol types. Finally, we derive monthly mean AODs by averaging all clear-sky aerosol profiles within each month over the three target regions. Although aerosol extinction coefficients within about 200 m of the surface are considered to be uncertain despite the application of quality filters (NASA CALIPSO team, 2011), we include them for completeness but exercise with caution when interpreting variations in AODs < 200 m. It should be noted that CALIPSO AOD is reported at a different wavelength (532 nm) from those used in the MISR and MODIS products (555 nm and 550 nm, respectively); this slight wavelength difference is not expected to affect our conclusions regarding AOD seasonal variations. Another caveat is that the monthly mean AOD from different sensors is calculated based on different sets of days, since MODIS provides near-daily global coverage while MISR and CALIPSO do not. We only use in our analysis monthly AOD averaged across 10 years and all grids/retrievals within three rather large regions (i.e., EUS, WEU, or ECC). In this case, the impact of the sampling issue is expected to be much smaller than that on the AOD retrieval in an individual month at a specific location.

168 2.2 AERONET and surface $PM_{2.5}$ data

169 We use AOD observations from AERONET to compare with the AOD seasonal
170 variations derived from satellite datasets. AERONET sunphotometers directly measure AOD at
171 seven wavelengths (approximately 340, 380, 440, 500, 675, 870, and 1020 nm) with an estimated
172 uncertainty of 0.01-0.02 (Holben et al., 2001; Eck et al., 1999), which is much smaller than the
173 uncertainties associated with satellite measurements (Kahn et al., 2010; Levy et al., 2010;
174 Schuster et al., 2012). Therefore, we consider AERONET as "ground truth" for AOD temporal
175 variations. We adopt the AERONET Level 2 Version 2.0 direct-sun measurements of spectral
176 AODs, which are subsequently interpolated to 550 nm using a second-order polynomial fit to
177 ln(AOD) vs. ln(wavelength) as recommended by Eck et al. (1999). A fundamental difference
178 between satellite and AERONET AOD observations is that a satellite acquires data at a single
179 overpass time (or spread over 7 minutes for MISR's nine views) and over an extended spatial
180 area in the case of MISR and MODIS, whereas AERONET obtains a time series of point data at
181 each surface station. To match coincident measurements, the AERONET AOD retrievals for
182 each site are averaged within a 2 h window centered on the satellite overpass times (about 10:30
183 for MISR and MODIS/Terra, and 13:30 for MODIS/Aqua and CALIPSO, depending on site
184 location), and compared with the satellite AOD retrievals in a 1° × 1° grid box (consistent with
185 the grids used in the MODIS Level 3 products) that contains the corresponding AERONET site.
186 Only those days for which a satellite overpasses an AERONENT site are used in the
187 comparisons. Since AOD variation has a large spatial correlation length of 40-400 km (Anderson
188 et al., 2003), spatial averaging over a 1° × 1° grid should not bias the seasonal variations of AOD
189 but has the benefit of increase the number of data points with valid AOD retrievals that are used
190 in the comparisons. To assure data quality, only the AERONET sites that span at least 5 years

with at least 10 months of valid data in each year are included in the comparison. After screening, 28, 54, and 13 sites are used in our analysis of the EUS, WEU, and ECC regions.

To provide additional information on the seasonal variations of satellite-observed aerosol loadings near the surface, we obtain surface $PM_{2.5}$ concentrations from several observational networks over the three target regions. Hourly $PM_{2.5}$ concentrations for 225 sites over the EUS region are achieved from the Air Quality System (AQS), which is a large observational database containing ambient air pollution data collected by the United States Environmental Protection Agency (USEPA), as well as state, local, and tribal air pollution control agencies in the United States (USEPA, 2017). For the ECC region, we obtain hourly $PM_{2.5}$ concentrations from the Ministry of Environmental Protection of China (MEP, http://datacenter.mep.gov.cn/), which provides continuous measurements at 496 sites located in 74 major cities in China. Hourly/daily $PM_{2.5}$ concentrations for 52 sites over the WEU region are taken from the European Monitoring and Evaluation Programme (EMEP). Similar to the processing of AERONET data, we only include sites whose data span ≥ 5 years with ≥ 10 months of data in each year, except in the case of the ECC region where at least 2 years' data are required because the $PM_{2.5}$ concentrations have been only publicly available since January 2013.

3 Results and Discussion

3.1 Seasonal variations of column AOD

Figure 2 illustrates the monthly variations in column AOD observed by MISR, MODIS/Terra, MODIS/Aqua, and CALIPSO during 2007-2016 in the three target regions. For consistency with the products from MISR and MODIS, only clear-sky daytime CALIPSO profiles are used to calculate the lidar-based monthly means. All satellite-borne sensors show that AOD in the EUS region is the highest in summer and lowest in winter, though CALIPSO

reports a noticeably smaller difference between the summer and winter extrema compared with the other three satellite instruments. For the WEU and ECC regions, MISR, MODIS/Terra, and MODIS/Aqua also reveal consistent seasonal patterns in which AOD peaks in spring and/or summer and reaches its lowest valley in winter. CALIPSO, however, shows little intra-annual variation in AOD, with small peaks occurring in spring and fall.

In view of the substantial differences between CALIPSO and the other three sensors, we compare satellite retrieved AOD seasonal variations with point-based ground measurements from AERONET (Fig. 3). As in other studies, AERONET data are treated as "ground truth" for column AOD due to its smaller uncertainty compared with satellite data (Kahn et al., 2010; Levy et al., 2010; Schuster et al., 2012; Fan et al., 2018). Figure 3 shows that, in all three regions, the AOD seasonal variations measured by AERONET are similar to those retrieved by MISR, MODIS/Terra, and MODIS/Aqua, but are quite different from CALIPSO data. Reasons for the differences between CALIPSO and other sensors will be discussed in Section 3.2. Considering the high accuracy of AERONET, AOD probably peaks in summer/spring and dips in winter. The higher AOD in summer is probably explained by accelerated formation of secondary aerosols, including sulfate, nitrate, ammonium, and secondary organic aerosol (SOA), as a result of stronger radiation and higher temperature in summer. Another possible reason is the higher RH in summer which favors the hygroscopic growth of aerosols (Liu et al., 2012; Zheng et al., 2017).

While relative pattern of AOD seasonal variations from observations of MISR, MODIS/Terra, and MODIS/Aqua are similar to each other and to those of AERONET, the magnitude of AOD observed by these sensors shows remarkable discrepancies. The MISR-retrieved AOD agrees well with the AERONET observations in EUS and WEU regions (Fig. 3). In the ECC region, however, MISR underestimates the AERONET AOD, probably because there

is less signal from the surface at higher AOD, which creates ambiguity that can result in the algorithm assigning too much of the top-of-atmosphere radiance to the surface (i.e., a higher surface albedo), thereby underestimating the AOD (Kahn et al., 2010). The MODIS/Terra and MODIS/Aqua significantly overestimate the AERONET AOD in EUS and WEU regions, and slightly overestimate the AERONET AOD in the ECC region, which is consistent with the evaluation results of Remer et al. (2005). This overestimation is largely attributed to the systematic positive bias at low AOD, likely attributed to an instrument calibration issue or an improper representation of surface reflectance at certain locations and seasons (Remer et al., 2005). The much smaller overestimation in the ECC region is explained by the fact that the MODIS AOD is not overestimated or even underestimated at the high AOD range, probably due to insufficient light absorption in the aerosol models (Remer et al., 2005).

3.2 Seasonal variations of aerosol loadings as a function of height

In addition to column AOD, the climatic effects of aerosols are also strongly dependent on their vertical distribution. To explore intra-annual variations in aerosol vertical profile, Fig. 4 presents CALIPSO-observed monthly variations of AOD as a function of height in the three target regions. A striking pattern is that the AOD seasonal variations are dramatically different at lower and upper heights. Over the WEU and ECC regions, AODs of the vertical layers below 800 m generally peak in winter, while those above 800 m peak in summer/spring. As a result, the CALIPSO-observed column AOD for these two regions presents a rather uniform seasonal pattern. For the EUS region, the maximum AOD above 800 m also occurs in summer; however, AOD below 800 m shows two peaks, one in summer and the other in winter. The integration of various layers thus yields a nearly unimodal distribution with maximum occurring in summer.

To provide an independent evaluation of the CALIPSO-observed AOD variations at lower heights, we examine the seasonal variations of near-surface $PM_{2.5}$ concentrations at hundreds of surface monitor locations within the three target regions. The aerosol extinction coefficient, and hence AOD at lower heights is affected by not only the particle mass concentrations, but also aerosol type (absorbing vs. nonabsorbing aerosols, coarse-mode vs. fine-mode aerosols) and meteorological parameters such as RH, wind speed and direction, and planetary boundary layer height (Zheng et al., 2017). Nevertheless, previous studies have reported fairly good correlations between extinction coefficient/low level AOD and $PM_{2.5}$ concentrations (Cheng et al., 2013; Zheng et al., 2017). For this reason, it is reasonable to qualitatively compare the seasonal variation patterns of near-surface $PM_{2.5}$ concentrations and low-level AOD. Figure 5 shows that, over the ECC and WEU regions, surface $PM_{2.5}$ concentrations are largest in winter and smallest in summer. In the EUS region, the maximum $PM_{2.5}$ concentration occurs in summer and a second maximum occurs in winter. These trends are generally consistent with the seasonal variations of AOD at low heights, implying that CALIPSO data can generally capture the seasonal changes in low-level aerosol abundance.

The aerosol vertical distribution is an important factor in reconciling CALIPSO and other sensors with regard to AOD seasonal variations. MISR, MODIS, and AERONET all measure column-integrated AOD using spectroradiometers, whereas CALIOP is an active lidar which estimates vertically-resolved AOD based on vertical profiles of attenuated backscatter. By comparing CALIPSO with the Atmospheric Radiation Measurement (ARM) program's ground-based Raman lidars, Thorsen et al. (2017) showed that CALIPSO does not detect all relatively significant aerosols due to insufficient detection sensitivity, and that the fraction of aerosols detected in the upper air is much smaller than that near the ground surface because the upper-

level aerosols tend to be optically thin. Therefore, the CALIPSO-observed AOD seasonal variations are significantly weighted toward lower heights. Specifically, over WEU and ECC regions, the unimodal AOD distributions with a summer peak at higher levels are largely counteracted by the opposite seasonal variations at lower levels, resulting in rather uniform seasonal variations of column AOD. For the EUS regions, due to the bimodal AOD distribution at lower heights, the summer peak in column AOD variations remain but the difference between peak and valley is smaller than implied by the observations of MISR and MODIS. In this sense, although the integrated CALIPSO column AOD does not agree well with AERONET, it does provide valuable information with respect to intra-annual variations of AOD at specific height ranges.

Why are the AOD seasonal variations different between the lower and upper atmosphere? The atmosphere in winter is generally more stable and vertical mixing is weaker, therefore more aerosols, particularly primary aerosols, are confined to lower heights, resulting in the peak of low-level AOD in winter (Guo et al., 2016; Liu et al., 2012; Zheng et al., 2017). At higher levels, the maximum AOD in summer can be explained by two reasons: (1) more aerosols, especially primary aerosols, are transported to the upper level in summer due to stronger vertical mixing (Guo et al., 2016; Liu et al., 2012; Zheng et al., 2017), and (2) secondary aerosol formation is more rapid in summer because of stronger radiation and higher temperature, and much of the secondary aerosols are produced in the upper air (de Reus et al., 2000; Minguillon et al., 2015; Heald et al., 2005). In addition, the seasonal variations of AOD at different vertical levels may also be influenced by the variations of RH which affects the hygroscopic growth (Liu et al., 2012; Zheng et al., 2017) as well as the seasonal patterns of inter-regional transport of aerosols (Tian et al., 2017).

305 3.3 Seasonal variations of aerosol types

306 Besides column AOD and vertical profiles, another factor influencing aerosol climate
307 impact is aerosol type (i.e., partitioning by size and chemical composition). The MISR and
308 CALIPSO products classify aerosols based on distinct principles of measurement and retrieval
309 algorithms. Analysis of the two datasets in combination can potentially lead to a deeper
310 understanding of the factors driving temporal variations of aerosol type. Figures 6 and 7 illustrate
311 the seasonal variations of AODs for various aerosol types retrieved by MISR and CALIPSO,
312 respectively. As discussed in Section 3.2, relative variability in CALIPSO-derived AOD at
313 different height ranges appears to be more reliable than integrated column AOD, therefore we
314 show aerosol types below and above 800 m separately in Fig. 7.

315 MISR distributes AODs into three size ranges, i.e., small (< 0.7 μm diameter), medium
316 (0.7-1.4 μm diameter), and large (> 1.4 μm diameter). Among the major constituents of ambient
317 aerosols, which include primary aerosols (dust, sea-spray aerosols, and primary anthropogenic
318 aerosols) and secondary aerosols (sulfate, nitrate, ammonium, and SOA), dust and sea-spray
319 aerosols are predominantly coarse particles and secondary aerosols are dominated by very fine
320 particles, while primary anthropogenic aerosols span a large size range, leading to a mean size
321 intermediate between dust/sea-spray and secondary constituents (Seinfeld and Pandis, 2006). Fig.
322 6 indicates that the small-size AOD is much larger in spring/summer than in winter over all
323 regions, whereas large-size AOD generally shows rather uniform distributions, except for the
324 ECC region where a peak occurs in late winter/early spring. The high small-size AOD in summer
325 is probably due to accelerated secondary aerosol formation and enhanced hygroscopic growth, as
326 described in Section 3.1. In contrast, AOD of primary anthropogenic aerosols should be less
327 influenced by seasonal effects, which partly accounts for the rather uniform distributions of

large-size AOD. Additionally, the changes in large-size AOD are also affected by other aerosol components including dust and sea-spray aerosols, as discussed below.

In contrast to MISR's partitioning of aerosol type by size, shape, and absorption, the CALIPSO-retrieved aerosol types (Fig. 7) are characterized by emission source. Particles associated with anthropogenic air pollution (polluted continental and polluted dust) comprise the dominant type in all three regions. At higher levels, the maximum AOD of polluted continental/dust aerosols occurs in spring/summer, while the maximum occurs in winter at lower levels (plus a second maximum in summer in EUS), in accordance with the seasonal variations of total AOD at different heights, as discussed in Section 3.2. With regard to dust and clean marine (sea-spray) aerosols, the AOD in the EUS region does not show an obvious seasonal pattern. In the WEU region, AOD of dust aerosols peaks in summer, consistent with previous surface-based observational studies which show that dust events in Europe predominantly occur during summer due to transport from the Sahara region (Stafoggia et al., 2016). The AOD of dust above 800 m is much larger than that below 800 m, supporting the conclusion that dust aerosols in WEU mainly originate from long range transport. Since the dust AOD has a quite large inter-annual variation (denoted by the error bars in Fig. 7), we use the Student's t-test to demonstrate the statistical significance of the seasonal variations shown above. The dust AOD in summer is statistically larger than that in any other season at the 0.05 level, indicating the robustness of the peak in summer. Contrary to dust, the AOD of sea-spray aerosols in WEU is much higher in winter than in summer, probably because winter is the relative windy season with large low pressure systems over the Atlantic Ocean and the North Sea (Manders et al., 2009). The offset of the opposite variation trends in dust and sea-spray aerosols partly accounts for the rather uniform distributions of large-size AOD (see Fig. 6). Over the ECC region, sea-spray aerosols make a

351 negligible contribution to total AOD. The dust AOD is much larger in spring than in any other
352 season (significant at the 0.05 level), which is tied to the outburst of springtime Gobi desert dust
353 storms (China Meteorological Administration, 2012). The high dust AOD explains the peak in
354 large-size AOD in spring over the ECC region (see Fig. 6).

355 Smoke aerosols are predominantly located above 800 m. Over the EUS and WEU regions,
356 smoke aerosols present a unimodal distribution with maximum occurring in summer. The
357 differences between smoke AOD in summer and the other three seasons are all statistically
358 significant at the 0.05 level, except for the difference between summer and spring over the WEU
359 region, which is statistically significant at the 0.10 level. In the ECC region, the smoke AOD
360 follows a bimodal distribution with peaks occurring in March and August and valleys occurring
361 in May and December. The differences between either of the peak months and either of the
362 valley months are statistically significant at the 0.05 level. MISR's independent retrieval of
363 absorbing AOD (Fig. 6) presents a similar seasonal pattern (statistically significant at the 0.05
364 level) as the CALIPSO smoke AOD. In fact, smoke consists of a larger fraction of absorbing
365 aerosols (Dubovik et al., 2002), such as BC and light-absorbing organic aerosol (Kirchstetter and
366 Thatcher, 2012), as compared to other aerosol types. The variability of MISR absorbing AOD
367 (shown in the right Y-axis of Fig. 6) is about 0.002-0.005, while the variability of smoke AOD
368 from CALIPSO is about 0.01-0.03. The smoke AOD includes the contributions of both the
369 absorbing and scattering portions. The MISR absorbing AOD, which is calculated using total
370 AOD × (1 – single scattering albedo), represents only the absorbing portion but includes
371 contributions from aerosol types other than smoke (Bull et al., 2011). Considering that the single
372 scattering albedo of smoke is about 0.80-0.94 (Dubovik et al., 2002), the MISR absorbing AOD
373 and CALIPSO smoke AOD are consistent in the order of magnitude. For the preceding reasons,

374 the seasonal patterns of smoke and absorbing aerosols acts as a cross-validation and strengthens
375 the reliability of the observed trends. Over the EUS and WEU regions, the largest smoke AOD in
376 summer could be explained by the highest emissions from forest and grassland fires (van der
377 Werf et al., 2017). Over the ECC region, an additional peak occurs in March because agricultural
378 residue burning makes a substantial contribution to total smoke emissions (van der Werf et al.,
379 2017), and such burning takes place more frequently in March due to burning of crop residues
380 left on the fields from the previous growing season (Shon, 2015).

381 3.4 Diurnal variations of height- and type-resolved AODs

382 CALIPSO provides both daytime and nighttime aerosol retrievals, giving an opportunity
383 to analyze aerosol diurnal variations. Care must be exercised in interpreting the CALIPSO-
384 observed diurnal variability because CALIPSO's detection sensitivity is lower during daytime
385 due to interference from sunlight. As a result, the difference between daytime and nighttime
386 AODs represents an overall effect of both actual and artificial diurnal variability. In this section,
387 we identify variation patterns that are most likely real, in spite of the possible effects of
388 measurement artifacts.

389 Figure 8 shows the differences between nighttime and daytime total and height-resolved
390 AODs (nighttime minus daytime values). The sign of the difference depends on the relative
391 importance of two competing factors: a more stable atmosphere at night favors the accumulation
392 of aerosols, whereas stronger photochemical reactions enhance aerosol loading during the day.
393 Fig. 8 reveals that nighttime AODs tend to be smaller than daytime AODs in winter. In contrast,
394 during summer and/or spring, nighttime AODs are higher than (WEU and ECC) or similar to
395 (EUS) the daytime values. More precisely, the difference between nighttime and daytime AODs
396 is significantly more positive in summer. This pattern is applicable to both AODs < 800 m and >

800 m. It is unlikely to be attributable to the difference in CALIPSO's detection sensitivity, which presumably exerts similar effects in all seasons. It should be noted, however, that we cannot fully exclude the effects of measurement artifacts, the quantification of which require further investigations using more accurate measurement techniques. A probable reason for more positive nighttime-daytime AOD difference in summer is that the diurnal temperature range, which is defined as the difference between the maximum and minimum temperatures in a day, is larger in summer (Ruschy et al., 1991; Jackson and Forster, 2010; Sun et al., 2006), giving rise to a larger difference in nighttime and daytime AODs due to a more stable nighttime atmosphere compared to a more unstable daytime atmosphere.

We further illustrate the differences between nighttime and daytime AODs of major aerosol types (Fig. 9). Smoke AOD is much higher in the nighttime than in the daytime. Considering that the emission rates of smoke aerosols is likely to be similar at different time of the day, the higher nighttime smoke AOD is probably the result of increased atmospheric stability at night, allowing the aerosols to accumulate. On the contrary, dust AOD is usually higher in the daytime, which may be tied to higher near-surface wind speed in the day (He et al., 2013; He et al., 2012; Hasson et al., 1990). The diurnal variations of polluted continental/dust aerosols vary according to season and height, and likely depend on the relative roles of more stable atmosphere at night and more active chemical reactions in the day. The type-dependent diurnal variations should mainly be representative of actual conditions, as such different variations as a function of aerosols type are unlikely explained by instrument detection sensitivity.

Atmos. Chem. Phys. Discuss., https://doi.org/10.5194/acp-2018-110
Manuscript under review for journal Atmos. Chem. Phys.
Discussion started: 12 April 2018

4 Conclusions and implications

This study investigated the seasonal and diurnal variations of aerosol column loading, vertical distribution, and particle types using multiple satellite and ground-based observational datasets during 2007-2016 over EUS, WEU, and ECC regions. Retrievals from MISR and MODIS reveal that column AOD in all three regions peaks in spring/summer and reaches its low in winter, which is consistent with observations from AERONET. This seasonal pattern is probably explained by accelerated formation of secondary aerosols in spring/summer due to stronger insolation and higher temperature. In contrast, CALIPSO shows a much weaker seasonal variability in column AOD, probably because CALIPSO-retrieved AOD is weighted toward lower heights since some thin aerosol layers in high levels are undetected due to insufficient detection sensitivity. Despite the discrepancy in integrated column AOD, CALIPSO does provide valuable information with respect to intra-annual variations of AOD as a function of height. Over the WEU and ECC regions, AODs of the vertical layers below 800 m generally peak in winter, while those above 800 m mostly peak in summer. For the EUS region, the maximum AOD above 800 m also occurs in summer; however, AOD below 800 m shows two peaks, one in summer and the other in winter. The seasonal variations of AOD at low heights are consistent with seasonal patterns of measured surface $PM_{2.5}$ concentrations.

When aerosols are binned into different size ranges, the small-size AOD is much larger in spring/summer than in winter over all three regions. Large-size AOD generally shows rather uniform distributions, except for the ECC region where a peak occurs in spring, consistent with the largest dust AOD in this season. When aerosols are classified according to sources, the aerosols associated with anthropogenic air pollution (as well as mixtures of anthropogenic pollution and dust) are the dominant type in all three regions. AOD of polluted aerosols has a

similar seasonal pattern as total AOD. Dust and clean marine aerosols in the WEU region peak in summer and winter, respectively, whereas they do not show an obvious seasonal pattern in the EUS region. Smoke aerosols, which CALIPSO indicates are predominantly located at heights above 800 m, present an obvious unimodal distribution with maximum occurring in summer over EUS and WEU regions, and a bimodal distribution with peaks in August and March over the ECC region. This pattern is in good agreement with the seasonal variations of absorbing AOD derived from MISR.

Regarding diurnal variations, the difference between nighttime and daytime AODs (nighttime minus daytime) is more positive in summer than in winter, which is likely explained by larger diurnal temperature range in summer. Smoke AOD is much higher in the nighttime, when the atmosphere is more stable, than in the daytime. On the contrary, dust AOD is usually higher in the daytime, when higher winds speeds enable a greater abundance of particles to become airborne.

The combination of multiple satellite and ground-based observations facilitate a systematic and deeper understanding of the seasonal and diurnal variations of aerosols, particularly their vertical and type distribution. Comparison of multiple measurement and retrieval methodologies enables reducing the uncertainties in the estimation of aerosol direct effects by providing improved information about aerosol vertical and type distributions, which significantly affect the aerosol-induced scattering and absorption of radiation. More importantly, the intra-annual variations of vertical distributions and types of aerosols are important for understanding their impact on atmospheric dynamics, cloud fields, and precipitation production. Many studies (Chen et al., 2017; Bond et al., 2013) have shown that BC and dust can either enhance or inhibit convection and hence cloud fields, depending on their vertical locations,

464 which are very different from the effects of non-absorbing aerosols (Ramanathan et al., 2005;
465 Fan et al., 2008; Massie et al., 2016). Finally, the data and variation patterns presented in this
466 study can be used to evaluate and improve model simulations, with the ultimate goal of
467 improving model assessment of the climatic and health effects of aerosols.

468

469 **Acknowledgments**

470 This study was supported by the MISR project at the Jet Propulsion Laboratory,
471 California Institute of Technology, under contract with NASA, NASA CCST program, and NSF
472 AGS-1701526. We acknowledge Michael J. Garay, Jason L. Tackett, and Ali H. Omar for their
473 valuable comments and suggestions. All data needed to evaluate the conclusions are present in
474 the paper.

475

476 **References**

477 Albrecht, B. A.: Aerosols, Cloud Microphysics, and Fractional Cloudiness, Science, 245, 1227-1230, DOI
478 10.1126/science.245.4923.1227, 1989.
479 Anderson, T. L., Charlson, R. J., Winker, D. M., Ogren, J. A., and Holmen, K.: Mesoscale variations of tropospheric
480 aerosols, J. Atmos. Sci., 60, 119-136, Doi 10.1175/1520-0469(2003)060<0119:Mvota>2.0.Co;2, 2003.
481 Bond, T. C., Doherty, S. J., Fahey, D. W., Forster, P. M., Berntsen, T., DeAngelo, B. J., Flanner, M. G., Ghan, S.,
482 Kaercher, B., Koch, D., Kinne, S., Kondo, Y., Quinn, P. K., Sarofim, M. C., Schultz, M. G., Schulz, M.,
483 Venkataraman, C., Zhang, H., Zhang, S., Bellouin, N., Guttikunda, S. K., Hopke, P. K., Jacobson, M. Z.,
484 Kaiser, J. W., Klimont, Z., Lohmann, U., Schwarz, J. P., Shindell, D., Storelvmo, T., Warren, S. G., and
485 Zender, C. S.: Bounding the role of black carbon in the climate system: A scientific assessment, J. Geophys.
486 Res-Atmos., 118, 5380-5552, 10.1002/jgrd.50171, 2013.
487 Bull, M., Matthews, J., McDonald, D., Menzies, A., Moroney, C., Mueller, K., Paradise, S., and Smyth, M.: MISR
488 Data Products Specifications Revision S, available at
489 https://eosweb.larc.nasa.gov/sites/default/files/project/misr/DPS_v50_RevS.pdf, Jet Propulsion Laboratory,
490 California Institute of Technology, 2011.
491 Chen, D., Liu, Z. Q., Davis, C., and Gu, Y.: Dust radiative effects on atmospheric thermodynamics and tropical
492 cyclogenesis over the Atlantic Ocean using WRF-Chem coupled with an AOD data assimilation system,
493 Atmos. Chem. Phys., 17, 7917-7939, 10.5194/acp-17-7917-2017, 2017.
494 Cheng, Z., Wang, S. X., Jiang, J. K., Fu, Q. Y., Chen, C. H., Xu, B. Y., Yu, J. Q., Fu, X., and Hao, J. M.: Long-term
495 trend of haze pollution and impact of particulate matter in the Yangtze River Delta, China, Environ. Pollut.,
496 182, 101-110, 10.1016/j.envpol.2013.06.043, 2013.
497 China Meteorological Administration: Sand-dust weather almanac 2010, China Meteorological Press, Beijing, 2012.

498 de Reus, M., Strom, J., Curtius, J., Pirjola, L., Vignati, E., Arnold, F., Hansson, H. C., Kulmala, M., Lelieveld, J.,
499 and Raes, F.: Aerosol production and growth in the upper free troposphere, J. Geophys. Res-Atmos., 105,
500 24751-24762, 10.1029/2000jd900382, 2000.
501 Diner, D. J., Beckert, J. C., Reilly, T. H., Bruegge, C. J., Conel, J. E., Kahn, R. A., Martonchik, J. V., Ackerman, T.
502 P., Davies, R., Gerstl, S. A. W., Gordon, H. R., Muller, J. P., Myneni, R. B., Sellers, P. J., Pinty, B., and
503 Verstraete, M. M.: Multi-angle Imaging SpectroRadiometer (MISR) - Instrument description and experiment
504 overview, IEEE. T. Geosci. Remote., 36, 1072-1087, 10.1109/36.700992, 1998.
505 Dubovik, O., Holben, B., Eck, T. F., Smirnov, A., Kaufman, Y. J., King, M. D., Tanre, D., and Slutsker, I.:
506 Variability of absorption and optical properties of key aerosol types observed in worldwide locations, J.
507 Atmos. Sci., 59, 590-608, 10.1175/1520-0469(2002)059<0590:voaaop>2.0.co;2, 2002.
508 Eck, T. F., Holben, B. N., Reid, J. S., Dubovik, O., Smirnov, A., O'Neill, N. T., Slutsker, I., and Kinne, S.:
509 Wavelength dependence of the optical depth of biomass burning, urban, and desert dust aerosols, J. Geophys.
510 Res-Atmos., 104, 31333-31349, 10.1029/1999jd900923, 1999.
511 Fan, J. W., Zhang, R. Y., Tao, W. K., and Mohr, K. I.: Effects of aerosol optical properties on deep convective
512 clouds and radiative forcing, J. Geophys. Res-Atmos., 113, 10.1029/2007jd009257, 2008.
513 Fan, X. H., Xia, X. A., and Chen, H. B.: Can MODIS Detect Trends in Aerosol Optical Depth Over Land?,
514 Advances in Atmospheric Sciences, 34, 1-11, 2018.
515 Garrett, T. J., and Zhao, C. F.: Increased Arctic cloud longwave emissivity associated with pollution from mid-
516 latitudes, Nature, 440, 787-789, 10.1038/nature04636, 2006.
517 Gu, Y., Liou, K. N., Xue, Y., Mechoso, C. R., Li, W., and Luo, Y.: Climatic effects of different aerosol types in
518 China simulated by the UCLA general circulation model, J. Geophys. Res-Atmos., 111,
519 10.1029/2005jd006312, 2006.
520 Guan, H., Schmid, B., Bucholtz, A., and Bergstrom, R.: Sensitivity of shortwave radiative flux density, forcing, and
521 heating rate to the aerosol vertical profile, J. Geophys. Res-Atmos., 115, 10.1029/2009jd012907, 2010.
522 Guo, J. P., Miao, Y. C., Zhang, Y., Liu, H., Li, Z. Q., Zhang, W. C., He, J., Lou, M. Y., Yan, Y., Bian, L. G., and
523 Zhai, P.: The climatology of planetary boundary layer height in China derived from radiosonde and reanalysis
524 data, Atmos. Chem. Phys., 16, 13309-13319, 10.5194/acp-16-13309-2016, 2016.
525 Hasson, A. M., Al-Hamadani, N. I., and Al-Karaghouli, A. A.: Comparison between measured and calculated
526 diurnal variations of wind speeds in northeast Baghdad, Solar & Wind Technoloqy, 7, 481-487, 1990.
527 He, Y. P., McFarlane, N. A., and Monahan, A. H.: The Influence of Boundary Layer Processes on the Diurnal
528 Variation of the Climatological Near-Surface Wind Speed Probability Distribution over Land, J. Climate., 25,
529 6441-6458, 10.1175/jcli-d-11-00321.1, 2012.
530 He, Y. P., Monahan, A. H., and McFarlane, N. A.: Diurnal variations of land surface wind speed probability
531 distributions under clear-sky and low-cloud conditions, Geophys. Res. Lett., 40, 3308-3314,
532 10.1002/grl.50575, 2013.
533 Heald, C. L., Jacob, D. J., Park, R. J., Russell, L. M., Huebert, B. J., Seinfeld, J. H., Liao, H., and Weber, R. J.: A
534 large organic aerosol source in the free troposphere missing from current models, Geophys. Res. Lett., 32,
535 L18809, DOI 10.1029/2005gl023831, 2005.
536 Holben, B. N., Tanre, D., Smirnov, A., Eck, T. F., Slutsker, I., Abuhassan, N., Newcomb, W. W., Schafer, J. S.,
537 Chatenet, B., Lavenu, F., Kaufman, Y. J., Castle, J. V., Setzer, A., Markham, B., Clark, D., Frouin, R.,
538 Halthore, R., Karneli, A., O'Neill, N. T., Pietras, C., Pinker, R. T., Voss, K., and Zibordi, G.: An emerging
539 ground-based aerosol climatology: Aerosol optical depth from AERONET, J. Geophys. Res-Atmos., 106,
540 12067-12097, 10.1029/2001jd900014, 2001.
541 Huang, L., Jiang, J. H., Tackett, J. L., Su, H., and Fu, R.: Seasonal and diurnal variations of aerosol extinction
542 profile and type distribution from CALIPSO 5-year observations, J. Geophys. Res-Atmos., 118, 4572-4596,
543 10.1002/jgrd.50407, 2013.
544 IPCC: Climate Change 2013: The Physical Science Basis. Contribution of Working Group I to the Fifth Assessment
545 Report of the Intergovernmental Panel on Climate Change, edited by: Stocker, T. F., Qin, D., Plattner, G.-K.,
546 Tignor, M., Allen, S. K., Boschung, J., Nauels, A., Xia, Y., Bex, V., and Midgley, P. M., Cambridge
547 University Press, Cambridge, United Kingdom and New York, NY, USA, 1535 pp., 2013.
548 Jackson, L. S., and Forster, P. M.: An Empirical Study of Geographic and Seasonal Variations in Diurnal
549 Temperature Range, J. Climate., 23, 3205-3221, 10.1175/2010jcli3215.1, 2010.
550 Johnson, B. T., Shine, K. P., and Forster, P. M.: The semi-direct aerosol effect: Impact of absorbing aerosols on
551 marine stratocumulus, Quarterly Journal of the Royal Meteorological Society, 130, 1407-1422,
552 10.1256/qj.03.61, 2004.

553 Johnson, B. T., Heese, B., McFarlane, S. A., Chazette, P., Jones, A., and Bellouin, N.: Vertical distribution and
554 radiative effects of mineral dust and biomass burning aerosol over West Africa during DABEX, J. Geophys.
555 Res-Atmos., 113, 10.1029/2008jd009848, 2008.
556 Kahn, R., Banerjee, P., and McDonald, D.: Sensitivity of multiangle imaging to natural mixtures of aerosols over
557 ocean, J. Geophys. Res-Atmos., 106, 18219-18238, 10.1029/2000jd900497, 2001.
558 Kahn, R. A., Gaitley, B. J., Martonchik, J. V., Diner, D. J., Crean, K. A., and Holben, B.: Multiangle Imaging
559 Spectroradiometer (MISR) global aerosol optical depth validation based on 2 years of coincident Aerosol
560 Robotic Network (AERONET) observations, J. Geophys. Res-Atmos., 110, 10.1029/2004jd004706, 2005.
561 Kahn, R. A., Gaitley, B. J., Garay, M. J., Diner, D. J., Eck, T. F., Smirnov, A., and Holben, B. N.: Multiangle
562 Imaging SpectroRadiometer global aerosol product assessment by comparison with the Aerosol Robotic
563 Network, J. Geophys. Res-Atmos., 115, 10.1029/2010jd014601, 2010.
564 Kahn, R. A., and Gaitley, B. J.: An analysis of global aerosol type as retrieved by MISR, J. Geophys. Res-Atmos.,
565 120, 4248-4281, 10.1002/2015jd023322, 2015.
566 Kim, S. W., Yoon, S. C., Kim, J., and Kim, S. Y.: Seasonal and monthly variations of columnar aerosol optical
567 properties over east Asia determined from multi-year MODIS, LIDAR, and AERONET Sun/sky radiometer
568 measurements, Atmos. Environ., 41, 1634-1651, 10.1016/j.atmosenv.2006.10.044, 2007.
569 King, M. D., Menzel, W. P., Kaufman, Y. J., Tanre, D., Gao, B. C., Platnick, S., Ackerman, S. A., Remer, L. A.,
570 Pincus, R., and Hubanks, P. A.: Cloud and aerosol properties, precipitable water, and profiles of temperature
571 and water vapor from MODIS, IEEE. T. Geosci. Remote., 41, 442-458, 10.1109/Tgrs.2002.808226, 2003.
572 Kirchstetter, T. W., and Thatcher, T. L.: Contribution of organic carbon to wood smoke particulate matter absorption
573 of solar radiation, Atmos. Chem. Phys., 12, 6067-6072, 10.5194/acp-12-6067-2012, 2012.
574 Lelieveld, J., Evans, J. S., Fnais, M., Giannadaki, D., and Pozzer, A.: The contribution of outdoor air pollution
575 sources to premature mortality on a global scale, Nature, 525, 367-+, 10.1038/nature15371, 2015.
576 Levy, R. C., Remer, L. A., Kleidman, R. G., Mattoo, S., Ichoku, C., Kahn, R., and Eck, T. F.: Global evaluation of
577 the Collection 5 MODIS dark-target aerosol products over land, Atmos. Chem. Phys., 10, 10399-10420,
578 10.5194/acp-10-10399-2010, 2010.
579 Li, S. S., Yu, C., Chen, L. F., Tao, J. H., Letu, H., Ge, W., Si, Y. D., and Liu, Y.: Inter-comparison of model-
580 simulated and satellite-retrieved componential aerosol optical depths in China, Atmos. Environ., 141, 320-
581 332, 10.1016/j.atmosenv.2016.06.075, 2016.
582 Liu, J. J., Zheng, Y. F., Li, Z. Q., Flynn, C., and Cribb, M.: Seasonal variations of aerosol optical properties, vertical
583 distribution and associated radiative effects in the Yangtze Delta region of China, J. Geophys. Res-Atmos.,
584 117, 10.1029/2011jd016490, 2012.
585 Ma, X. Y., Yu, F. Q., and Quaas, J.: Reassessment of satellite-based estimate of aerosol climate forcing, J. Geophys.
586 Res-Atmos., 119, 10.1002/2014jd021670, 2014.
587 Manders, A. M. M., Schaap, M., Jozwicka, M., van Arkel, F., Weijers, E. P., and Matthijsen, J.: The contribution of
588 sea salt to PM10 and PM2.5 in the Netherlands. Netherlands Research Program on Particulate Matter, Report
589 500099004, http://www.pbl.nl/sites/default/files/cms/publicaties/500099004.pdf, 2009.
590 Mao, K. B., Ma, Y., Xia, L., Chen, W. Y., Shen, X. Y., He, T. J., and Xu, T. R.: Global aerosol change in the last
591 decade: An analysis based on MODIS data, Atmos. Environ., 94, 680-686, 10.1016/j.atmosenv.2014.04.053,
592 2014.
593 Massie, S. T., Delano, J., Bardeen, C. G., Jiang, J. H., and Huang, L.: Changes in the shape of cloud ice water
594 content vertical structure due to aerosol variations, Atmos. Chem. Phys., 16, 6091-6105, 10.5194/acp-16-
595 6091-2016, 2016.
596 Matthias, V., Balis, D., Bosenberg, J., Eixmann, R., Iarlori, M., Komguem, L., Mattis, I., Papayannis, A.,
597 Pappalardo, G., Perrone, M. R., and Wang, X.: Vertical aerosol distribution over Europe: Statistical analysis
598 of Raman lidar data from 10 European Aerosol Research Lidar Network (EARLINET) stations, J. Geophys.
599 Res-Atmos., 109, 10.1029/2004jd004638, 2004.
600 McCormick, R. A., and Ludwig, J. H.: Climate Modification by Atmospheric Aerosols, Science, 156, 1358-&, DOI
601 10.1126/science.156.3780.1358, 1967.
602 Mehta, M., Singh, R., Singh, A., Singh, N., and Anshumali: Recent global aerosol optical depth variations and
603 trends - A comparative study using MODIS and MISR level 3 datasets, Remote. Sens. Environ., 181, 137-
604 150, 10.1016/j.rse.2016.04.004, 2016.
605 Mielonen, T., Arola, A., Komppula, M., Kukkonen, J., Koskinen, J., de Leeuw, G., and Lehtinen, K. E. J.:
606 Comparison of CALIOP level 2 aerosol subtypes to aerosol types derived from AERONET inversion data,
607 Geophys. Res. Lett., 36, 10.1029/2009gl039609, 2009.

608 Minguillon, M. C., Brines, M., Perez, N., Reche, C., Pandolfi, M., Fonseca, A. S., Amato, F., Alastuey, A., Lyasota,
609 A., Codina, B., Lee, H. K., Eun, H. R., Ahn, K. H., and Querol, X.: New particle formation at ground level
610 and in the vertical column over the Barcelona area, Atmos. Res., 164, 118-130,
611 10.1016/j.atmosres.2015.05.003, 2015.
612 NASA CALIPSO team: CALIPSO Quality Statements Lidar Level 3 Aerosol Profile Monthly Products Version
613 Release: 1.00,
614 https://eosweb.larc.nasa.gov/PRODOCS/calipso/Quality_Summaries/CALIOP_L3AProProducts_1-00.html,
615 access: Nov 23, 2017, 2011.
616 Niu, F., and Li, Z. Q.: Systematic variations of cloud top temperature and precipitation rate with aerosols over the
617 global tropics, Atmos. Chem. Phys., 12, 8491-8498, 10.5194/acp-12-8491-2012, 2012.
618 Ramanathan, V., Crutzen, P. J., Kiehl, J. T., and Rosenfeld, D.: Atmosphere - Aerosols, climate, and the
619 hydrological cycle, Science, 294, 2119-2124, 10.1126/science.1064034, 2001.
620 Ramanathan, V., Chung, C., Kim, D., Bettge, T., Buja, L., Kiehl, J. T., Washington, W. M., Fu, Q., Sikka, D. R.,
621 and Wild, M.: Atmospheric brown clouds: Impacts on South Asian climate and hydrological cycle, P. Natl.
622 Acad. Sci. USA., 102, 5326-5333, 10.1073/pnas.0500656102, 2005.
623 Ramanathan, V., Ramana, M. V., Roberts, G., Kim, D., Corrigan, C., Chung, C., and Winker, D.: Warming trends in
624 Asia amplified by brown cloud solar absorption, Nature, 448, 575-U575, 10.1038/nature06019, 2007.
625 Remer, L. A., Kaufman, Y. J., Tanre, D., Mattoo, S., Chu, D. A., Martins, J. V., Li, R. R., Ichoku, C., Levy, R. C.,
626 Kleidman, R. G., Eck, T. F., Vermote, E., and Holben, B. N.: The MODIS aerosol algorithm, products, and
627 validation, J. Atmos. Sci., 62, 947-973, Doi 10.1175/Jas3385.1, 2005.
628 Rosenfeld, D., Lohmann, U., Raga, G. B., O'Dowd, C. D., Kulmala, M., Fuzzi, S., Reissell, A., and Andreae, M. O.:
629 Flood or drought: How do aerosols affect precipitation?, Science, 321, 1309-1313, 10.1126/science.1160606,
630 2008.
631 Ruschy, D. L., Baker, D. G., and Skaggs, R. H.: Seasonal-variation in daily temperature ranges, J. Climate., 4, 1211-
632 1216, 10.1175/1520-0442(1991)004<1211:svidtr>2.0.co;2, 1991.
633 Schuster, G. L., Vaughan, M., MacDonnell, D., Su, W., Winker, D., Dubovik, O., Lapyonok, T., and Trepte, C.:
634 Comparison of CALIPSO aerosol optical depth retrievals to AERONET measurements, and a climatology for
635 the lidar ratio of dust, Atmos. Chem. Phys., 12, 7431-7452, 10.5194/acp-12-7431-2012, 2012.
636 Seinfeld, J. H., and Pandis, S. N.: Atmospheric Chemistry and Physics, from air pollution to climate change, John
637 Wiley & Sons, Inc., Hoboken, New Jersey, 2006.
638 Shindell, D. T., Faluvegi, G., Koch, D. M., Schmidt, G. A., Unger, N., and Bauer, S. E.: Improved Attribution of
639 Climate Forcing to Emissions, Science, 326, 716-718, 10.1126/science.1174760, 2009.
640 Shon, Z. H.: Long-term variations in PM2.5 emission from open biomass burning in Northeast Asia derived from
641 satellite-derived data for 2000-2013, Atmos. Environ., 107, 342-350, 10.1016/j.atmosenv.2015.02.038, 2015.
642 Song, C. K., Ho, C. H., Park, R. J., Choi, Y. S., Kim, J., Gong, D. Y., and Lee, Y. B.: Spatial and Seasonal
643 Variations of Surface PM10 Concentration and MODIS Aerosol Optical Depth over China, Asia-Pac. J.
644 Atmos. Sci., 45, 33-43, 2009.
645 Song, S. K., Shon, Z. H., and Park, Y. H.: Diurnal and seasonal characteristics of the optical properties and direct
646 radiative forcing of different aerosol components in Seoul megacity, Sci. Total. Environ., 599, 400-412,
647 10.1016/j.scitotenv.2017.04.195, 2017.
648 Stafoggia, M., Zauli-Sajani, S., Pey, J., Samoli, E., Alessandrini, E., Basagana, X., Cernigliaro, A., Chiusolo, M.,
649 Demaria, M., Diaz, J., Faustini, A., Katsouyanni, K., Kelessis, A. G., Linares, C., Marchesi, S., Medina, S.,
650 Pandolfi, P., Perez, N., Querol, X., Randi, G., Ranzi, A., Tobias, A., Forastiere, F., Angelini, P., Berti, G.,
651 Bisanti, L., Cadum, E., Catrambone, M., Davoli, M., de' Donato, F., Gandini, M., Grosa, M., Ferrari, S.,
652 Pelosini, R., Perrino, C., Pietrodangelo, A., Pizzi, L., Poluzzi, V., Priod, G., Rowinski, M., Scarinzi, C.,
653 Stivanello, E., Dimakopoulou, K., Elefteriadis, K., Kelessis, A., Maggos, T., Michalopoulos, N., Pateraki, S.,
654 Petrakakis, M., Rodopoulou, S., Sypsa, V., Agis, D., Alguacil, J., Artinano, B., Barrera-Gomez, J., de la
655 Rosa, J., Fernandez, R., Jacquemin, B., Karanasiou, A., Ostro, B., Salvador, P., Sanchez, A. M., Sunyer, J.,
656 Bidondo, M., Declercq, C., Le Tertre, A., Lozano, P., Pascal, L., Pascal, M., and Grp, M.-P. S.: Desert Dust
657 Outbreaks in Southern Europe: Contribution to Daily PM10 Concentrations and Short-Term Associations
658 with Mortality and Hospital Admissions, Environ. Health. Persp., 124, 413-419, 10.1289/ehp.1409164, 2016.
659 Sun, D., Kafatos, M., Pinker, R. T., and Easterling, D. R.: Seasonal variations in diurnal temperature range from
660 satellites and surface observations, IEEE. T. Geosci. Remote., 44, 2779-2785, 10.1109/tgrs.2006.871895,
661 2006.

662 Thorsen, T. J., Ferrare, R. A., Hostetler, C. A., Vaughan, M. A., and Fu, Q.: The impact of lidar detection sensitivity
663 on assessing aerosol direct radiative effects, Geophys. Res. Lett., 44, 9059-9067, 10.1002/2017gl074521,
664 2017.
665 Tian, P. F., Cao, X. J., Zhang, L., Sun, N. X., Sun, L., Logan, T., Shi, J. S., Wang, Y., Ji, Y. M., Lin, Y., Huang, Z.
666 W., Zhou, T., Shi, Y. Y., and Zhang, R. Y.: Aerosol vertical distribution and optical properties over China
667 from long-term satellite and ground-based remote sensing, Atmos. Chem. Phys., 17, 2509-2523, 10.5194/acp-
668 17-2509-2017, 2017.
669 Twomey, S.: Influence of pollution on shortwave albedo of clouds, J. Atmos. Sci., 34, 1149-1152, 10.1175/1520-
670 0469(1977)034<1149:tiopot>2.0.co;2, 1977.
671 Unger, N., Shindell, D. T., Koch, D. M., and Streets, D. G.: Air pollution radiative forcing from specific emissions
672 sectors at 2030, J. Geophys. Res-Atmos., 113, 10.1029/2007jd008683, 2008.
673 USEPA: Air Quality System (AQS), https://www.epa.gov/aqs, access: Dec 15, 2017, 2017.
674 van der Werf, G. R., Randerson, J. T., Giglio, L., van Leeuwen, T. T., Chen, Y., Rogers, B. M., Mu, M. Q., van
675 Marle, M. J. E., Morton, D. C., Collatz, G. J., Yokelson, R. J., and Kasibhatla, P. S.: Global fire emissions
676 estimates during 1997-2016, Earth System Science Data, 9, 697-720, 10.5194/essd-9-697-2017, 2017.
677 Wang, J. D., Zhao, B., Wang, S. X., Yang, F. M., Xing, J., Morawska, L., Ding, A. J., Kulmala, M., Kerminen, V.
678 M., Kujansuu, J., Wang, Z. F., Ding, D. A., Zhang, X. Y., Wang, H. B., Tian, M., Petaja, T., Jiang, J. K., and
679 Hao, J. M.: Particulate matter pollution over China and the effects of control policies, Sci. Total. Environ.,
680 584, 426-447, 10.1016/j.scitotenv.2017.01.027, 2017.
681 Wang, S. X., Zhao, B., Cai, S. Y., Klimont, Z., Nielsen, C. P., Morikawa, T., Woo, J. H., Kim, Y., Fu, X., Xu, J. Y.,
682 Hao, J. M., and He, K. B.: Emission trends and mitigation options for air pollutants in East Asia, Atmos.
683 Chem. Phys., 14, 6571-6603, DOI 10.5194/acp-14-6571-2014, 2014.
684 Yu, H. B., Chin, M., Winker, D. M., Omar, A. H., Liu, Z. Y., Kittaka, C., and Diehl, T.: Global view of aerosol
685 vertical distributions from CALIPSO lidar measurements and GOCART simulations: Regional and seasonal
686 variations, J. Geophys. Res-Atmos., 115, 10.1029/2009jd013364, 2010.
687 Zhang, L., Li, Q. B., Gu, Y., Liou, K. N., and Meland, B.: Dust vertical profile impact on global radiative forcing
688 estimation using a coupled chemical-transport-radiative-transfer model, Atmos. Chem. Phys., 13, 7097-7114,
689 10.5194/acp-13-7097-2013, 2013.
690 Zhao, B., Jiang, J. H., Gu, Y., Diner, D., Worden, J., Liou, K. N., Su, H., Xing, J., Garay, M., and Huang, L.:
691 Decadal-scale trends in regional aerosol particle properties and their linkage to emission changes, Environ.
692 Res. Lett., 12, 054021, 10.1088/1748-9326/aa6cb2, 2017.
693 Zhao, B., Liou, K.-N., Gu, Y., Jiang, J. H., Li, Q., Fu, R., Huang, L., Liu, X., Shi, X., Su, H., and He, C.: Impact of
694 aerosols on ice crystal size, Atmos. Chem. Phys., 18, 1065-1078, DOI 10.5194/acp-18-1065-2018, 2018.
695 Zheng, C. W., Zhao, C. F., Zhu, Y. N., Wang, Y., Shi, X. Q., Wu, X. L., Chen, T. M., Wu, F., and Qiu, Y. M.:
696 Analysis of influential factors for the relationship between PM2.5 and AOD in Beijing, Atmos. Chem. Phys.,
697 17, 13473-13489, 10.5194/acp-17-13473-2017, 2017.
698

Atmos. Chem. Phys. Discuss., https://doi.org/10.5194/acp-2018-110
Manuscript under review for journal Atmos. Chem. Phys.
Discussion started: 12 April 2018

Atmospheric Chemistry and Physics Discussions

Figures

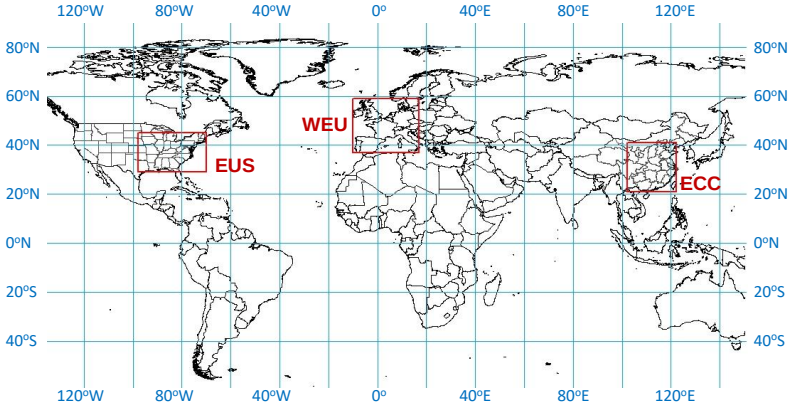

Figure 1. Target regions for this study: the Eastern United States (EUS), Western Europe (WEU), and Eastern and Central China (ECC).

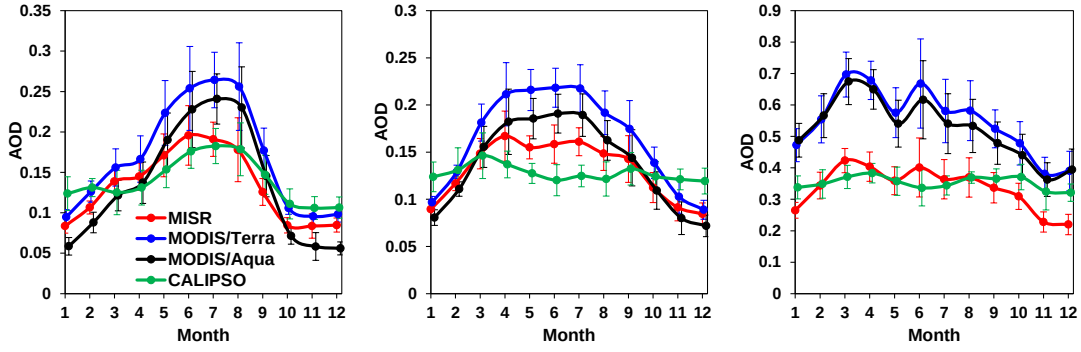

Figure 2. Monthly mean AOD observed by MISR, MODIS/Terra, MODIS/Aqua, and CALIPSO during 2007-2016 in (a) EUS, (b) WEU, and (c) ECC. For CALIPSO, only clear-sky daytime profiles are averaged in order to be consistent with the MISR and MODIS products. The error bars denote the standard deviation of the monthly mean AOD values obtained over all years. Note the different scales on the y-axes of the plots.

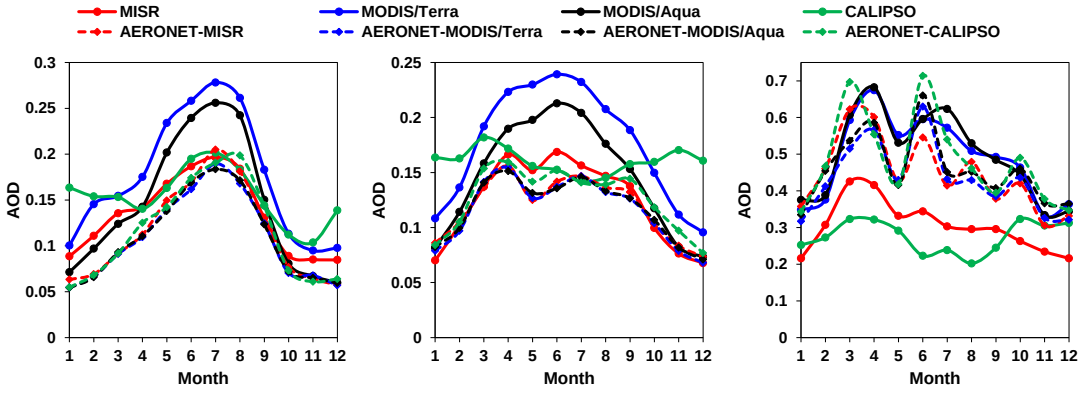

709 **Figure 3**. Monthly mean AOD observed by satellites and AERONET averaged across the
710 AERONET sites during 2007-2016 in (a) EUS, (b) WEU, and (c) ECC. The observations from
711 MISR, MODIS/Terra, MODIS/Aqua, and CALIPSO are averaged over 1°×1° grid boxes
712 containing the AERONET sites. The AERONET data are averaged within a 2 h window
713 centered on satellite overpass times. The numbers of AERONET sites included in analysis are
714 28, 54, and 13, in the EUS, WEU, and ECC regions, respectively. Since the four sensors
715 overpass a site in different days and different times of day, we separately calculate the
716 AERONET data matched to each sensor (denoted by "AERONET-×××"). The AERONET curves
717 matched to different sensors are close in EUS and WEU, partly because there are plenty of
718 sites in these two regions, and the discrepancy due to the sampling issue is therefore smoothed
719 out. In contrast, there are only 13 AERONET sites in ECC, so there exists larger discrepancy
720 between the AERONET data matched to different sensors. Note the different scales on the y-
721 axes of the plots.

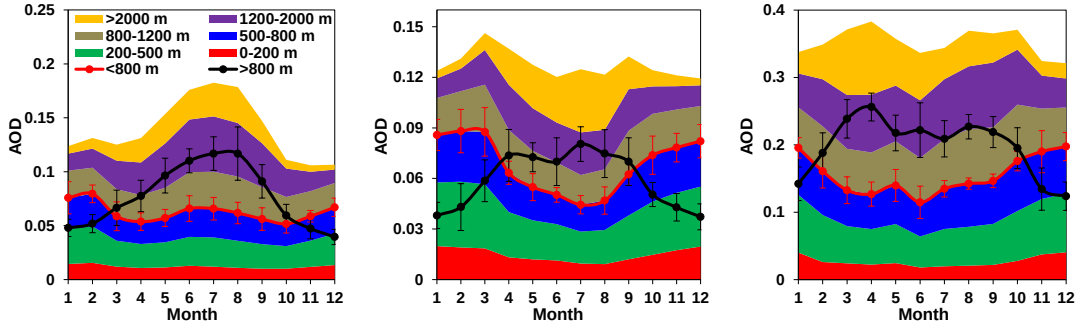

722 **Figure 4**. Monthly mean AOD as a function of height above ground level observed by CALIPSO
723 during 2007-2016 in (a) EUS, (b) WEU, and (c) ECC. Only clear-sky daytime profiles are
724 averaged in order to be consistent with the products of MISR and MODIS. The range of AOD
725 within a particular height range is depicted by the colored stacks. The integrated AODs for
726 heights below and above 800 m are shown as solid lines, for which the error bars are defined in
727 the same way as in Fig. 2. Note the different scales on the y-axes of the plots.

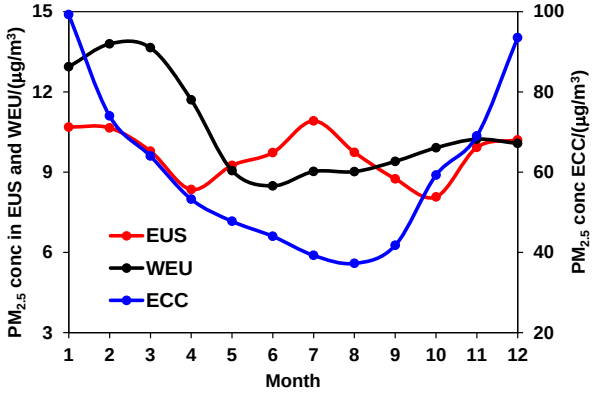

728
729 **Figure 5.** Monthly mean surface $PM_{2.5}$ concentrations during 2007-2016 in three target regions.
730 The numbers of observational sites included in averaging are 225, 52, and 496, in the EUS,
731 WEU, and ECC regions. Note the different scales on the y-axes for EUS/WEU and ECC.

Atmos. Chem. Phys. Discuss., https://doi.org/10.5194/acp-2018-110
Manuscript under review for journal Atmos. Chem. Phys.
Discussion started: 12 April 2018

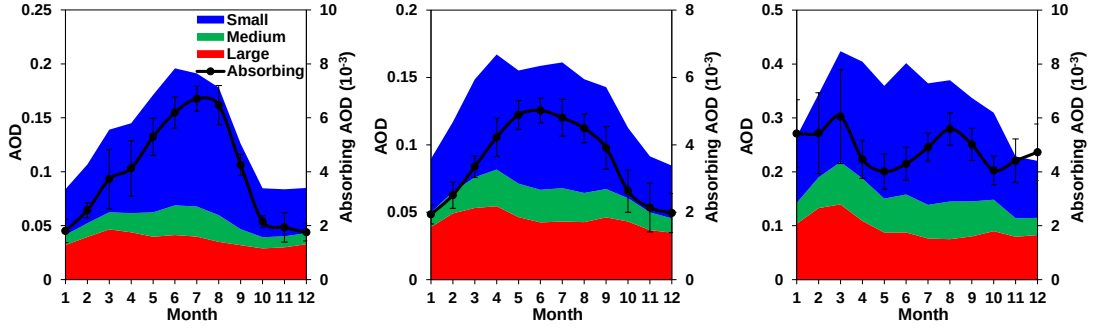

732 **Figure 6**. Monthly mean AOD of different aerosol types observed by MISR during 2007-2016 in
733 (a) EUS, (b) WEU, and (c) ECC. The size-resolved AODs are depicted by the colored stacks
734 (left Y-axis); the integration of the three size ranges yields total column AOD, as represented by
735 the upper edge of the blue color. The AOD of absorbing aerosols is shown as solid lines (right
736 Y-axis), for which the error bars are defined in the same way as in Fig. 2. Note the different
737 scales on the y-axes of the plots.

Atmos. Chem. Phys. Discuss., https://doi.org/10.5194/acp-2018-110
Manuscript under review for journal Atmos. Chem. Phys.
Discussion started: 12 April 2018

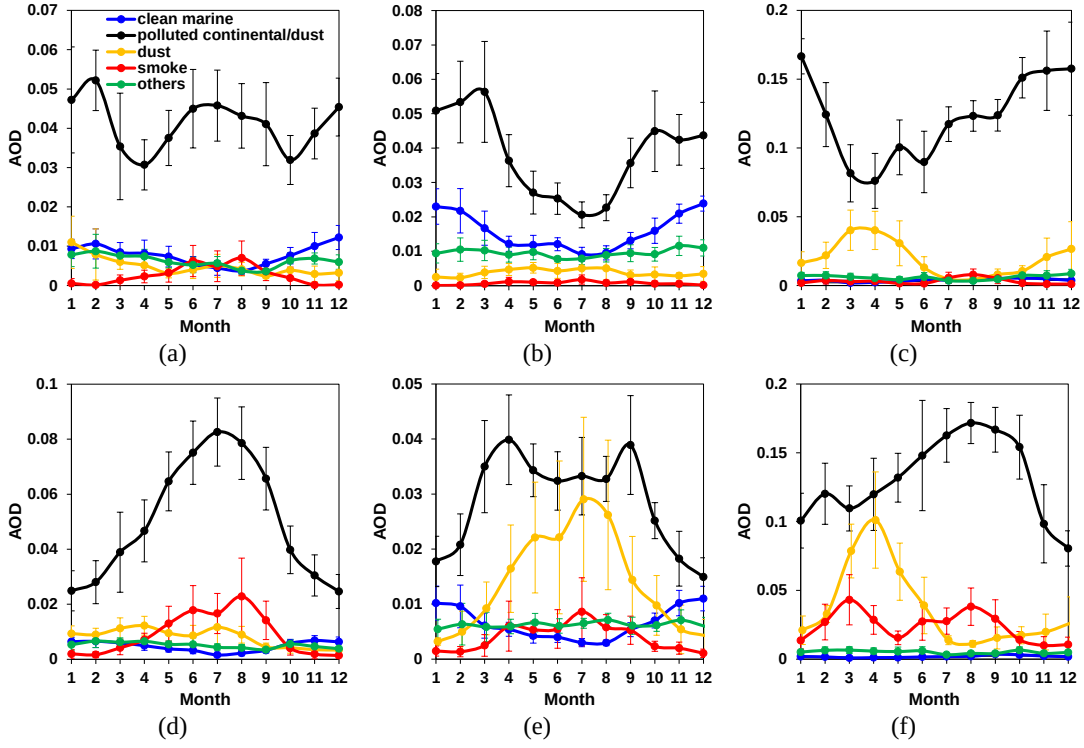

738 **Figure 7**. Monthly mean AOD of different aerosol types (a-c) below 800 m and (d-f) above
739 800 m observed by CALIPSO during 2007-2016 in (a, d) EUS, (b, e) WEU, and (c, f) ECC. Only
740 clear-sky daytime profiles are used in the averaging to be consistent with the products of MISR
741 and MODIS. The definition of error bars is the same as in Fig. 2. Note the different scales on the
742 y-axes of the plots.

Atmos. Chem. Phys. Discuss., https://doi.org/10.5194/acp-2018-110
Manuscript under review for journal Atmos. Chem. Phys.
Discussion started: 12 April 2018

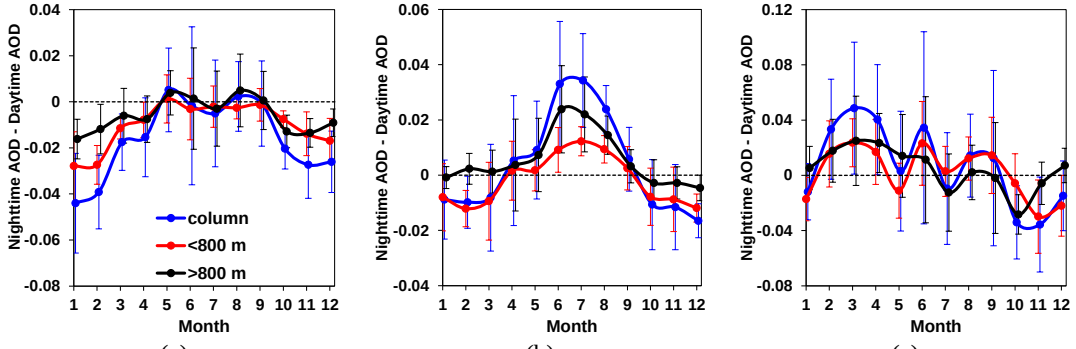

743 **Figure 8**. Differences between monthly mean nighttime and daytime AODs (including column
744 AODs, as well as AODs of aerosols located below 800 m and above 800 m) observed by
745 CALIPSO during 2007-2016 in (a) EUS, (b) WEU, and (c) ECC. Only clear-sky profiles are
746 included. The definition of error bars is the same as in Fig. 2. Note the different scales on the y-
747 axes of the plots.

Atmos. Chem. Phys. Discuss., https://doi.org/10.5194/acp-2018-110
Manuscript under review for journal Atmos. Chem. Phys.
Discussion started: 12 April 2018

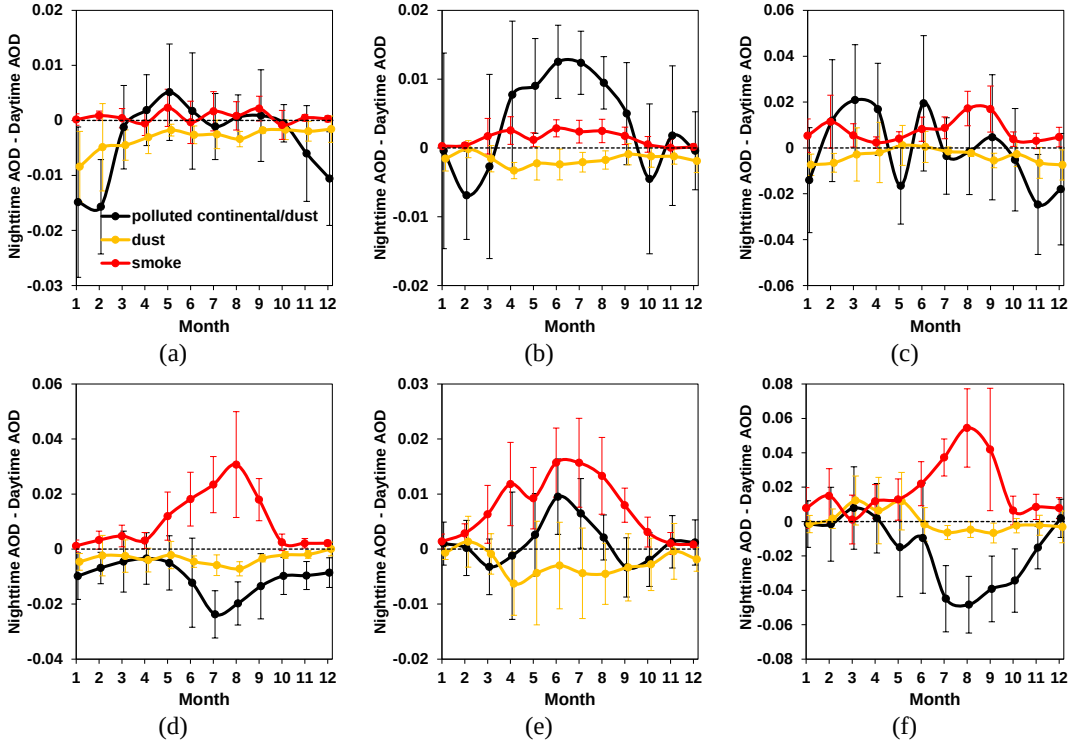

748 **Figure 9**. Differences between monthly mean nighttime and daytime AODs of different aerosol
749 types (a-c) below 800 m and (d-f) above 800 m observed by CALIPSO during 2007-2016 in (a,
750 d) EUS, (b, e) WEU, and (c, f) ECC. Only clear-sky profiles are included. The definition of error
751 bars is the same as in Fig. 2. Note the different scales on the y-axes of the plots.

752